PERGAMON

Control Engineering Practice 9 (2001) 933–945

CONTROL ENGINEERING PRACTICE

www.elsevier.com/locate/conengprac

Control of strip casting process: decentralization and optimal roll force control ☆

Keum-Shik Hong[a,*], Jeom-Goo Kim[b], Masayoshi Tomizuka[c]

[a] School of Mechanical Engineering, Pusan National University, 30 Changjeon-dong, Kumjeong-ku, Pusan, 609-735, South Korea
[b] Graduate College, Pusan National University, 30 Changjeon-dong, Kumjeong-ku, Pusan, 609-735, South Korea
[c] Mechanical Engineering Department, University of California, Berkeley, CA 94720-1740, USA

Received 9 May 2000; accepted 8 December 2000

Abstract

In this paper, modeling and control of a twin-roll strip caster are investigated. The control objectives are to achieve a constant strip thickness and to maintain a constant roll separating force. Mathematical models are derived by analyzing five critical areas: molten steel level in the pool, solidification process, roll separating force and torque, roll gap dynamics, and roll drive dynamics. A two-level control strategy is proposed. At low level, three local controllers regulate three subsystems independently. They are a variable structure controller for the molten steel level of the pool, an adaptive predictive controller for the roll gap, which is directly related to the strip thickness, and a two-degree-of-freedom robust servo controller for the roll speed. At high level, an H_2 optimal controller governs the interaction dynamics among subsystems and generates a reference signal to the local roll speed controller in the fashion that a constant roll separating force is maintained. In designing the high level controller, the complex strip casting dynamics is linearized at an operating point and parameter estimation and uncertainty quantification methods are used. Simulation results are provided.

Keywords: Strip casting process; Modeling; Feedback control; Decentralized control; Uncertainty quantification; H_2 optimal control

1. Introduction

The strip casting process is a new steel-strip production method, which combines two processes of continuous casting and hot rolling. As shown in Fig. 1, the molten liquid steel from the tundish is directly poured into the space made by two rotating rolls and side dams. Compared with the conventional continuous casting, the preliminary forming process using a mould is eliminated and the production line from molten liquid steel to final products is shortened. The strip casting method is currently considered as one of the two new emerging technologies, together with the COREX process, in the steel process industry.

For the continuous casting process, a number of advanced control techniques have been investigated by several researchers. Significant cost reduction and quality improvement have also been reported: Hesketh, Clements, and Williams (1993) applied an adaptive control technique for the mould level control of continuous steel slab casting. Graebe, Goodwin, and Elsley (1995) revealed various nonlinearities appearing in the continuous casting process and raised several critical issues that had to be solved in controller design and implementation. For the rolling process, a repetitive control approach to reject unknown periodic load disturbances due to the eccentricity of the rolls has also been reported by Manayathara, Tsao, Bentsman, and Ross (1996) and Garimella and Srinivasan (1996).

However, results on the strip casting are very rare. Bernhard, Enning, and Rake (1994) have investigated an optimal control for regulating the strip casting thickness for a laboratory scale pilot strip caster. Lee, Lee, Kim, and Lee (1996) have investigated a fuzzy controller for the stable start-up operation of a strip caster.

In this paper, a mathematical model and a two-level control of the twin-roll strip caster are investigated. The casting process is divided into five subparts for modeling

☆ This paper was not presented at any IFAC meeting.

*Corresponding author. Tel.: +82-51-510-2454; Fax: +82-51-514-0685.

E-mail addresses: kshong@hyowon.pusan.ac.kr (K.-S. Hong), jgkim92@hyowon.pusan.ac.kr (J.-G. Kim), tomizuka@me.berkeley.edu (M. Tomizuka).

0967-0661/01/$ - see front matter
PII: S0967-0661(01)00042-9

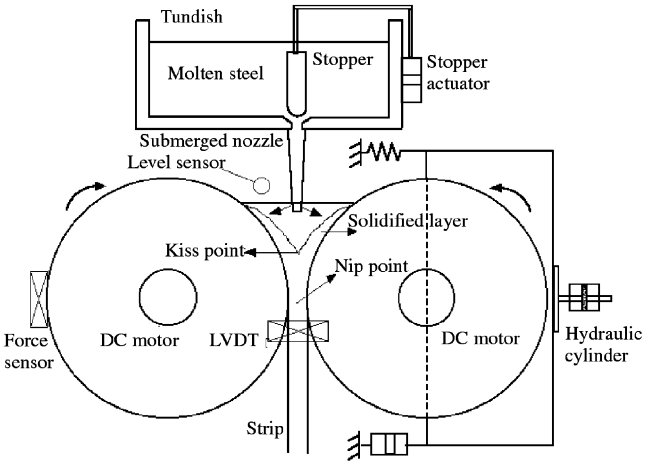

Fig. 1. A schematic diagram of the strip casting process.

and three subparts for control system design. The five subparts for modeling are the molten steel level dynamics of the pool, the solidification process of the molten steel in the pool, the roll separating force and torque relationship, the roll gap dynamics including hydraulic actuator dynamics, and the roll and DC motor dynamics. The three subparts for control system design are a roll gap positioning system, a roll drive system, and a molten steel level control system.

After a systematic analysis for the five subparts for modeling and three subparts for control system design, a two-level control structure is synthesized. The purposes of low-level control (local control) are to minimize the interference among subsystems and to simplify the structure of high-level control. The overall control performance of low-level controllers is supervised by a high-level controller which generates appropriate reference signals to the low-level controllers. It is also shown that the proposed control strategy is very effective for handling the complicated multi-variable nonlinear strip casting dynamics.

The control objectives of strip casting process are to obtain a uniform thickness of the strip and to maintain a constant roll separating force throughout the casting process in the presence of various disturbances. The uniform strip thickness is pursued by low-level controllers and the constant roll separating force is maintained by a high-level controller. The three low-level controllers include a variable structure controller for the molten steel level, an adaptive predictive controller for the roll gap, and a two-degree-of-freedom robust servo controller for the roll drive system. Each decentralized local controller treats the interaction among subsystems as a disturbance to the subsystem. On the other hand, the high-level roll separating force controller governs the strip casting dynamics and generates a reference signal to the local roll speed controller. Because the entire strip casting dynamics is very complicated, a manageable nominal model for the purpose of designing a high-level supervising controller is derived by linearizing the system dynamics at an operating point. Since the parameter values of this nominal model are not known, a recursive least squares estimation method is used to estimate these parameters. Then, the model errors, which include the unstructured uncertainty neglected in the modeling stage and the structured uncertainty in the parameter estimation stage, are quantified as magnitude bounds in the frequency domain. Finally, an H_2 robust controller is designed using the uncertainty bounds derived.

Contributions of this paper are as follows: first, the strip casting process is for the first time modeled by giving specific mathematical models for five subsystems. Second, a two-level control strategy for achieving a uniform thickness of the strip and minimal residual stress on the strip by applying constant roll separating force throughout the process is proposed. Third, individual local controllers are selected to best fit the nature of local dynamics and disturbances. Fourth, a genuine strategy for controlling the roll separating force is for the first time proposed.

This paper is structured as follows: in Section 2, mathematical models for the strip casting process are formulated. In Section 3, three local controllers are designed and then a high-level roll separating force controller is proposed by utilizing system identification and uncertainty quantification methods. Simulation results are given in Section 4. Finally, conclusions are stated in Section 5.

2. Strip casting process: modeling

Fig. 1 shows a schematic diagram of the strip casting process. The molten liquid steel is poured from the tundish into the pool made by two rotating rolls and two side dams. The bottom end of the nozzle, through which the molten steel comes down, is submerged in the pool not yet solidified. The flow rate of the molten steel into the pool is controlled by adjusting the height of the stopper. The temperature of roll surfaces is maintained by cooling water, which circulates through the inner pipes in the rolls. Thus, once the liquid steel hits the roll surface, it rapidly solidifies from outside to inside, and the solid layer gets thicker as the two rolls rotate. The intersection point of the two boundary lines separating liquid and solid states is called the "kiss point" and the narrowest part of the strip is called the "nip point". The roll gap between two rolls is adjusted by translating the right roll back and forth with an electro-hydraulic gap positioning system. The frame of the translating roll is guided by low friction linear bearings in the horizontal direction. The rotating velocity of each roll is controlled by a DC-motor. The measurement sensors used in this

work include one level sensor for the molten steel level, one loadcell for measuring the roll separating force, one LVDT for measuring the roll gap, and one resolver for measuring the roll speed.

The strip casting process is very complex. It is a multi-input and multi-output system and the dynamics involved are highly nonlinear. The roll force generation mechanism as well as the solidification process involves various types of uncertainties and disturbances. For a rigorous analysis of the process, the entire process is divided into five subparts as follows:

2.1. Molten steel level dynamics

Fig. 2 is a schematic diagram for analyzing the molten steel level dynamics of the pool. Let m be the total mass contained in the control volume made by two rotating drums and two side dams. The mass flow rate into the control volume is described by the continuity equation as follows:

$$\dot{m} = \dot{m}_i - \dot{m}_o, \tag{1}$$

where subscripts i and o stand for in and out, respectively. Let ϕ_L be the angle made by the horizontal line and the line segment heading to the level of the pool. Let $A = A(\phi_L)$ be the area of the cross section (vertical) of the control volume, which is a function of ϕ_L. Then, using the geometry in Fig. 2, the following relations are obtained:

$$m = \rho_2 LA, \tag{2}$$

$$A = R\left\{(2R + D)\sin\phi_L - \frac{R}{2}\sin(2\phi_L) - R\phi_L\right\},$$

where R and L are the radius and the width of a roll, respectively, D is the roll gap between two rolls, and ρ_2 is the average density of the material in the control volume. In exact sense, ρ_2 is time-varying. However, it is treated as a constant in this paper because it varies slowly compared to other mechanical dynamics.

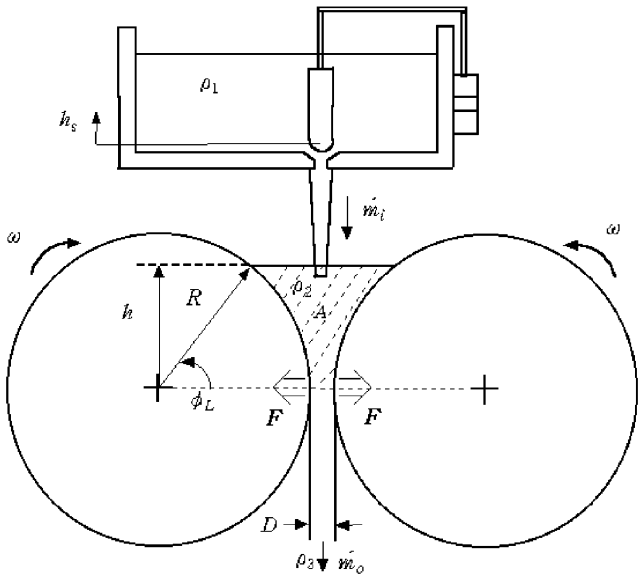

Fig. 2. A schematic for analyzing the molten steel level dynamics.

The mass flow rate out of the control volume is given by

$$\dot{m}_o = \rho_3 LRD\omega, \tag{3}$$

where ρ_3 is the density of the solid strip coming out of the control volume and ω is the angular velocity of the roll. And the liquid steel coming into the volume is described by the first order differential equation as follows:

$$\dot{m}_i = \frac{\rho_1 k_q}{\tau_s s + 1} h_s, \tag{4}$$

where h_s denotes the position of the stopper, ρ_1 is the density of the molten steel, k_q is a flow gain associated with the stopper geometry, and τ_s is a time constant. Both k_q and τ_s are determined from experiments.

Let $h = R\sin\phi_L$ be the molten steel level. Then, differentiating (2) and substituting (3) and (4) into (1), the following molten steel level dynamics is derived:

$$\rho_2 L\left\{2R + D - 2R\sqrt{1 - \left(\frac{h}{R}\right)^2}\right\}\dot{h} + \rho_2 Lh\dot{D} - \frac{\rho_1 k_q}{\tau_s s + 1} h_s + \rho_3 LRD\omega = 0. \tag{5}$$

In (5), the control input is h_s and ρ_2 is an uncertain parameter whose upper and lower values are bounded by ρ_1 and ρ_3, respectively. It is also noted that D and ω dynamics are treated as disturbances in the h dynamics, while they are coupled variables in view of the entire strip casting process. In Section 3.1.1 a variable structure controller for (5) is designed.

2.2. Modeling of solidification process

This section considers the dynamics of the kiss point. Since the roll force and torque are affected by the amount of solid steel accumulated in the control volume, an estimate of the depth of the kiss point is necessary to generate a uniform roll separating force. It is also noted that because the thermal processes are much slower than the mechanical dynamics, the heat transfer phenomena are not taken into account in this paper.

The growth of the solid layer in Fig. 3 can be described in two different ways. In Lagrangian description, in which the description is tagged on a moving particle, the thickness δ of the solidified layer can be described as

$$\delta(T) = C(T - \tau)^{\beta}, \tag{6}$$

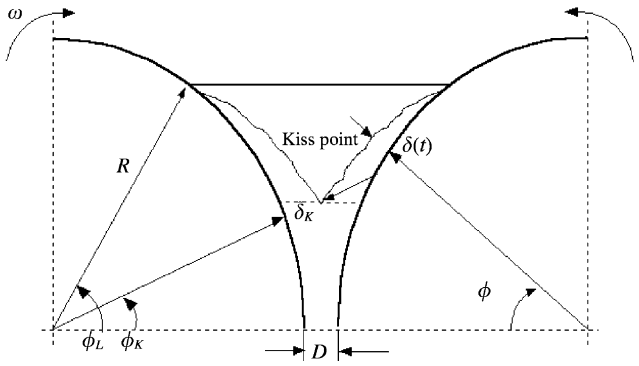

Fig. 3. Solidification process.

where T is the total elapsed time for which the solid particle has moved from the initial solidification point to the current stage, τ is a time delay that happens when the liquid temperature is higher than the solidification temperature, and C and β are coefficients determined by experiments. In particular, the thickness of the solidified layer at the kiss point is denoted by

$$\delta_K = C(T_K - \tau)^{\beta}, \tag{7}$$

where δ_K is the strip thickness at the kiss point and T_K is the traveling time of a solid particle from the roll surface to the kiss point. Note that T_K depends on the location of the kiss point (ϕ_K), the roll speed ω, and the molten steel level ϕ_L.

On the other hand, if the solidification process is observed in a fixed reference coordinate frame (Eulerian description), the thickness of the solid layer at the kiss point δ_K varies in time. Let $\phi_K(t)$ be the angle made by the horizontal line and the line segment to the kiss point at time t. Let $\phi_L(t - T_K)$ be the angle made by the horizontal line and the line segment to the level of the pool at T_K ahead of time. Then, the following relationship between the roll speed and T_K holds:

$$\phi_L(t - T_K) - \phi_K(t) = \int_{t - T_K}^{t} \omega(v)\,\mathrm{d}v, \tag{8}$$

where $\omega(t)$ is the roll rotating speed. And using the geometry in Fig. 3, the following equation between ϕ_K and δ_K at the kiss point is derived:

$$(R + \delta_K(t))\cos\phi_K(t) = R + \frac{D(t)}{2}. \tag{9}$$

Now, adopting the work of Bernhard et al. (1994), a differential equation for T_k (the reaching time to the kiss point) is derived. Substituting (7) into (9) yields

$$\{R + C(T_K(t) - \tau)^{\beta}\}\cos\phi_K = R + \frac{D(t)}{2}. \tag{10}$$

It is noted that if ϕ_K increases, the roll separating force increases. Therefore, it is desirable to keep ϕ_K as small as possible. Assuming that ϕ_K is relatively small, expand $\cos\phi_K$ in Taylor series up to the second order (if $\phi_K = 30^{\circ}$ is assumed, $\cos(\pi/6) = 0.8660$ and $1 - (\pi/6)^2/2 = 0.8629$. Therefore, the approximation, $\cos(\phi_K) \approx 1 - \phi_K^2/2$, is quite reasonable). Then, (10) becomes

$$\{R + C(T_K(t) - \tau)^{\beta}\}\left(1 - \frac{\phi_K^2(t)}{2}\right) = R + \frac{D(t)}{2}. \tag{11}$$

The differentiation of (8) and (11) in time yields

$$\dot{\phi}_L(t - T_K)(1 - \dot{T}_K) - \dot{\phi}_K = \omega(t) - \omega(t - T_K)(1 - \dot{T}_K), \tag{12}$$

$$C\beta(T_K(t) - \tau)^{\beta - 1}\dot{T}_K(t)\left(1 - \frac{\phi_K^2(t)}{2}\right) - \{R + C(T_K(t) - \tau)^{\beta}\}\phi_K(t)\dot{\phi}_K(t) = \frac{\dot{D}(t)}{2}. \tag{13}$$

Combining Eqs. (11)–(13) and omitting t in T_K, ϕ_K, and D for simplicity, a differential equation for T_K is finally derived as follows:

$$\dot{T}_K = \frac{\dot{\phi}_L(t - T_K) - \omega(t) + \omega(t - T_K) + g_2(D, T_K)\dot{D}}{\dot{\phi}_L(t - T_K) + \omega(t - T_K) + g_1(D, T_K)}, \tag{14}$$

where

$$g_1(D, T_K) = \frac{C\beta(T_K - \tau)^{\beta - 1}\dfrac{R + D/2}{R + C(T_K - \tau)^{\beta}}}{\left\{\sqrt{2}\sqrt{1 - \dfrac{R + D/2}{R + C(T_K - \tau)^{\beta}}}\right\}\{R + C(T_K - \tau)^{\beta}\}}$$

and

$$g_2(D, T_K) = \frac{1}{\left\{2\sqrt{2}\sqrt{1 - \dfrac{R + D/2}{R + C(T_K - \tau)^{\beta}}}\right\}\{R + C(T_K - \tau)^{\beta}\}}.$$

Remark 1. It is observed in (14) that three variables (ϕ_L, ω, and D) play the key role in estimating T_K. Once T_K is determined, the location of the kiss point ϕ_K can be decided from (11). Because the roll separating force is given as a function of ϕ_K, see Eq. (15) in Section 2.3 next, and the high level controller try to achieve a uniform roll separating force, the attempt to regulate these three variables by individual local controllers is justified.

2.3. Roll separating force and torque

Several empirical equations that describe the roll force and moment generated in hot rolling are available in the literature (Pietrzyk & Lenard, 1991, p. 53; Hesketh

et al., 1993). These empirical equations are derived by using the classical theory of plasticity analyzing the equilibrium status of an infinitesimal section. In this paper, the following roll separating force F and torque M derived using the elementary rolling theory are adopted (see Bernhard et al., 1994).

$$F = 2.4k_f LR^2 \frac{1-\cos\phi_K}{D+R(1-\cos\phi_K)}, \tag{15}$$

$$M = FR\frac{1}{\sqrt{2}}\sqrt{1-\cos\phi_K}, \tag{16}$$

where k_f is a constant that is characterized by the plasticity of the material.

2.4. Roll gap dynamics

Fig. 4 shows a schematic diagram of the roll-gap positioning system and the roll drive system. Each roll is rotated by a DC motor. To achieve a desired roll gap, the right roll frame is moved with a hydraulic actuator.

Let m_r, b_r and k_r be the mass, damping coefficient, and spring constant of the moving roll unit, respectively. Let D and F be the roll gap and roll separating force between two rolls. Let p_a and p_b be the supply and return pressures of the hydraulic system, respectively. Let $p_l = p_a - p_b$ and A_{cyl} be the pressure difference and the size of the hydraulic cylinder, respectively. Then, the following dynamic equation for the moving roll holds:

$$m_r\frac{\mathrm{d}^2D}{\mathrm{d}t^2} + b_r\frac{\mathrm{d}D}{\mathrm{d}t} + k_rD + F = A_{cyl}p_l. \tag{17}$$

Now, regarding the hydraulic subsystem, the flow rate into the cylinder, q, is assumed as

$$q = a_1 d - a_2 p_l, \tag{18}$$

where d is the servo valve spool position, and a_1 and a_2 are proportionality constants. The leakage flow across the valve spool and the compressibility of the fluid are all neglected. Neglecting further the dynamics of the servo valve spool, the spool position d in (18) is given as

$$d = K_i i, \tag{19}$$

where i is the current input to the servo valve and K_i is a constant. Utilizing the fact that $q = A_{cyl}\,\mathrm{d}D/\mathrm{d}t$, an input–output relation of the roll gap dynamics is derived as

$$m_r\frac{\mathrm{d}^2D}{\mathrm{d}t^2} + \left(b_r + \frac{A_{cyl}^2}{a_2}\right)\frac{\mathrm{d}D}{\mathrm{d}t} + k_rD = \frac{a_1A_{cyl}K_i}{a_2}i - A_{cyl}F. \tag{20}$$

Remark 2. Two things are noted. First, in (20) the interference from other subsystems is given in the form of F. It acts as a disturbance when the roll gap is regulated. Second, the actual strip thickness is not the same as the roll gap D, because there is a deformation resistance along the steel strip due to the roll separating force F. But, if the roll separating force is regulated at constant, a uniform deformation resistance can be assumed. So, the actual steel strip thickness is given by εD, where ε is a deformation ratio depending on the material.

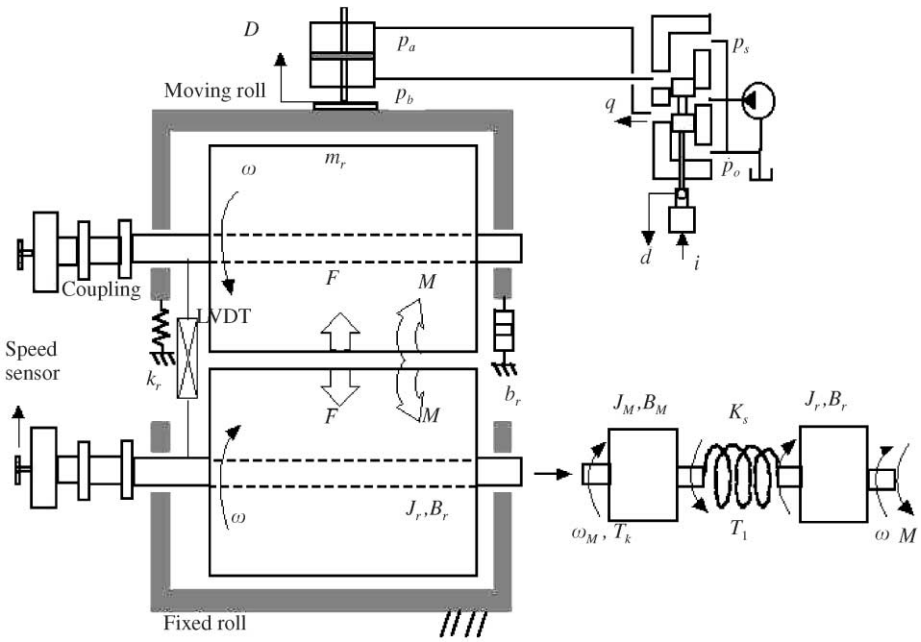

Fig. 4. Schematics for the roll gap positioning system and the roll drive system.

2.5. Roll drive dynamics

As shown in Fig. 4, the torsional dynamics exist in the roll drive system because of a large gear-ratio coupling. In this case, the drive system can be modeled as a two mass system with a torsional spring.

Table 1
System parameters used for simulations

Symbol	Description	Value
L	Width of a roll	1,300 mm
R	Radius of a roll	1,250 mm
ρ_1	Density of the molten steel	7244 kg/m^3
ρ_2	Average density of the steel	7250 kg/m^3
ρ_3	Density of the solid steel	7266 kg/m^3
K_q	Flow gain	0.1 m^2/s
τ_s	Time constant	0.5 s
C	Solidification coefficient	0.45 m/s
β	Solidification index	0.6
K_f	Roll separating force constant	5.03×10^{-6} kgf/mm^2
m_r	Mass of the moving roll	550 kg
k_r	Spring constant of the moving roll	100 N s/m
b_r	Damping coefficient of the moving roll	4.73×10^3 N/m
A_{cyl}	Size of the hydraulic cylinder	12.57×10^{-4} m^2
a_1	Proportionality constant	0.128 m^2/s
a_2	Proportionality constant	3.2756 m^3/s Pa
K_i	Current gain	1.587×10^{-2} m/A
K_T	Torque constant	2.05 N m/A
J_M	Inertia of the motor	4.016×10^{-2} kg m^2
B_M	Damping coefficient of the motor	0.015 N m s/rad
K_s	Torsional spring constant	2.15 N m/rad
J_r	Inertia of the main roll	300 kg m^2
R_g	Gear ratio	50
B_r	Damping coefficient of the main roll	0.1 N m s/rad

Since the bandwidth of the current controller is generally much wider than that of the speed controller, the current command input can be assumed to be equal to the motor armature current i_a. Then, the motor torque T_M is given by

$$T_M = K_T i_a \tag{21}$$

where K_T is the torque constant. According to Newton's second law, the dynamics of the roll drive subsystem is given by

$$T_M = J_M \dot{\omega}_M + B_M \omega_M + T_1, \tag{22}$$

$$T_1 = K_s(\theta_M - \theta),$$

$$T_1 = J_r \dot{\omega} + B_r \omega + M,$$

where J_M and B_M are the inertia and damping coefficient of the motor, K_s is a torsional spring constant, J_r and B_r are the inertia and damping coefficient of the main rolls, and M is the roll torque.

Finally, all the system parameters derived in Section 2, which will be used for simulations in Section 4, are tabulated in Table 1.

3. Control system design

Although the actual strip thickness is different from the size of the roll gap, it can be assumed that a constant roll gap and a constant roll separating force will lead to a constant strip thickness. The roll separating force and the water temperature inside the rolls can affect mechanical properties, particularly the residual stress, of the steel strip. In this paper, it is assumed that the cooling system is well maintained in the steady state environment. So, a simultaneous regulation of the roll

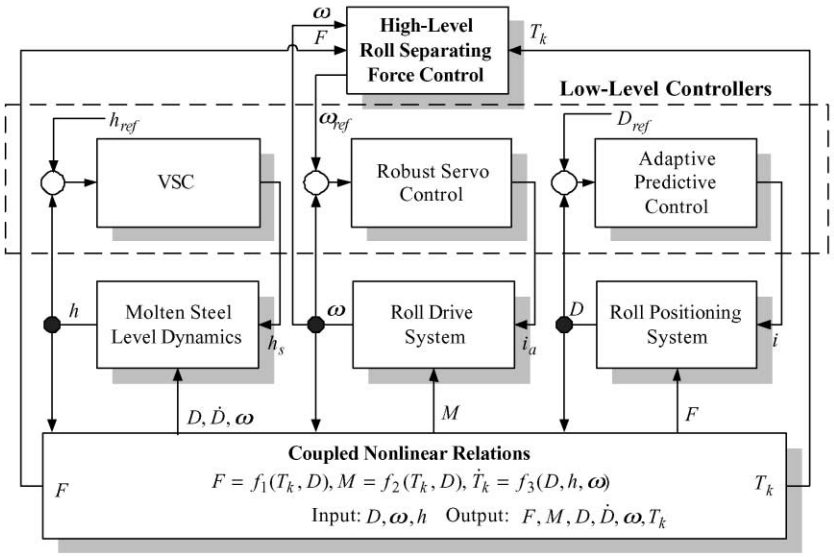

Fig. 5. Structure of the two-level control.

gap and the roll separating force will fulfill the control objectives of this paper.

The mathematical model developed in Section 2 is highly nonlinear involving empirical equations and various uncertainties. So, it is impossible to achieve the control objectives with a single controller. In this paper, a two-level control strategy is proposed.

As stated in Remark 1, the roll separating force can be maintained at a constant value by regulating three variables; ϕ_L, ω, and D. Therefore, it is desirable to have three local controllers to regulate their outputs by direct feedback and to run independently with their own robustness against interference from other parts. The interference from other parts should be treated as a disturbance in its own dynamics. But, because modeling uncertainties and external disturbances always exist, this decentralization strategy alone will not be sufficient to achieve a constant roll separating force. Therefore, a high-level controller, which governs the entire dynamics and provides reference signals to the local controllers, is needed. Because the start-up dynamics is more complex than the steady state dynamics, only a steady state high-level controller is investigated in this paper.

Fig. 5 shows a schematic for the proposed two-level control strategy. The regulated variables of three local control loops are the molten steel level h, the roll speed ω, and the strip thickness D. And, their control inputs are the stopper height h_s, the armature current command i_a to the motor, and the servo-valve current i. On the other hand, the regulated signal of the high-level control loop is the roll separating force F and its manipulated variable is the reference signal to the roll speed controller (ω_{ref}).

3.1. Local controllers

In this section, three decentralized controllers are designed: a molten steel level controller, a roll gap controller, and a roll speed controller. Each controller tracks its desired reference signal and the interaction with other parts is treated as disturbances.

3.1.1. Molten steel level control

From (5), the state equation of the molten steel level h is derived as follows:

$$\dot{h} = f(h;\ D, \dot{D}, \omega) + b(h;\ D)z, \tag{23a}$$

$$\dot{z} = -\frac{1}{\tau_s}z + \frac{1}{\tau_s}h_s, \tag{23b}$$

where

$$f(\cdot) = -\frac{\rho_3 LRD\omega + \rho_2 Lh\dot{D}}{\rho_2 L\left\{2R + D - 2R\sqrt{1 - \left(\frac{h}{R}\right)^2}\right\}},$$

$$b(\cdot) = -\frac{\rho_1 k_q}{\rho_2 L\left\{2R + D - 2R\sqrt{1 - \left(\frac{h}{R}\right)^2}\right\}}$$

and h_s is the stopper height. Since τ_s is small, $z \approx h_s$ may be assumed.

Observing (23a), the following several issues are recognized as potential impediments to achieve a desired molten steel level: (i) Nonlinear relationship of D, $\dot{D}$, and ω is due to the nonlinear geometry of the pool. (ii) ρ_2 cannot be measured and furthermore is also time-varying because the ratio of solid and liquid parts in the pool is changing. (iii) The flow rate k_q may be time-varying, because the submerged nozzle and the stopper may clog or their sizes may change due to wear and erosion.

In this subsection considering the above impediments, the variable structure control technique for regulating the molten steel level is proposed. A key idea is that the upper and lower bounds of $f(\cdot)$ and $b(\cdot)$ are known because the control variables of the roll gap and the roll speed controllers are set not to exceed some values and the bounds for ρ_2 and k_q are also known.

In order to make the output to track $h(t) = h_{ref}(t)$, where $h_{ref}(t)$ is the desired level, the following sliding surface ($s = 0$) and sliding condition are defined (Slotine & Li, 1991, p. 276).

$$s(t) = (\mathrm{d}/\mathrm{d}t + \lambda)\int_0^t \tilde{h}(\upsilon)\,\mathrm{d}\upsilon,$$

$$\frac{1}{2}\frac{\mathrm{d}}{\mathrm{d}t}s^2(t) \leqslant -\eta|s(t)|$$

where λ and η are strictly positive constants and $\tilde{h} = h - h_{ref}$. To achieve the sliding condition above and to handle an undesirable chattering, the following reaching law is used.

$$\dot{s}(t) = -ksat\left(\frac{s(t)}{\Phi}\right),$$

where Φ is the boundary layer thickness and sat is the saturation function. So the following control law is determined as

$$h_s(t) = \frac{1}{\hat{b}}\left\{-\hat{f} + \dot{h}_{ref}(t) - \lambda\tilde{h}(t) - ksat\left(\frac{s(t)}{\Phi}\right)\right\}, \tag{24}$$

where $\hat{f}$ and $\hat{b}$ are the estimated values. Also, a gain k is determined to assure the robustness in the presence of disturbances and parameter variations. The parameter values used in the simulations of Section 4 are: $\lambda = 4$,

$\Phi = 0.001$, and $k = 1.1$. For more detailed design scheme, (Slotine & Li, 1991) is referred.

3.1.2. Roll gap control

Taking the Laplace transform of (20), the transfer function from the armature current i to the roll gap D is given by

$$D(s) = \frac{\frac{a_1}{a_2}A_{cyl}K_i}{m_r s^2 + \left(b_r + \frac{A_{cyl}^2}{a_2}\right)s + k_r} i(s) - \frac{A_{cyl}}{m_r s^2 + \left(b_r + \frac{A_{cyl}^2}{a_2}\right)s + k_r} F(s). \quad (25)$$

Regarding (25), two facts are noted. First, the roll separating force F is a nonperiodic but smoothly changing disturbance in the D-dynamics, but this can be measured. Second, the parameter values are not known at the beginning, however, they will not vary significantly during operation. These two aspects motivate us the use of one-step ahead adaptive predictive control for the regulation of the roll gap at a constant value. To apply the adaptive predictive control, (25) is now converted to the discrete form as follows (Phillips & Nagle, 1997):

$$D(z) = \sum_{\substack{\text{at poles} \\ \text{of } D(s)}} \left[\text{residues of } D(s)\ \frac{1}{1 - z^{-1}e^{T_s s}}\right] = \frac{b_0 z}{z^2 + a_1 z + a_2} i(z) - \frac{c_0 z}{z^2 + a_1 z + a_2} F(z), \quad (26)$$

where T_s is a sampling period. Rearranging terms of (26), the following regression form is obtained:

$$D(k) = \phi^{\mathrm{T}}(k)\theta \quad (27)$$

where $\phi^{\mathrm{T}}(k) = [-D(k-1)\ -D(k-2)\ i(k-1) - F(k-1)]$ and $\theta^{\mathrm{T}} = [a_1\ a_2\ b_0\ c_0]$. Then, a recursive least squares estimation algorithm (Astrom & Wittenmark, 1995; Ljung, 1987) can be used to estimate θ. For parameter estimation, at least two sets of experiment, with and without the load, are recommended to enhance the validity of estimates. The estimated parameters are: $\hat{a}_1 = -0.4358$, $\hat{a}_2 = -0.441$, $\hat{b}_0 = 0.00316$, and $\hat{c}_0 = 0.007353$.

Finally, as a control law for changing the strip thickness, the one-step ahead predictive control is adopted as follows:

$$i(k) = \frac{\hat{b}_0}{\hat{b}_0^2 + \lambda_1}\{D_{ref}(k+1) + \hat{a}_1 D(k) + \hat{a}_2 D(k-1) + \hat{c}_0 F(k)\}, \quad (28)$$

where D_{ref} is the desired roll gap, F is the measured roll separating force, $\lambda_1 = 0.00001$, and the hated variables are the estimated parameters. The role of λ_1 is to prevent the singularity of the control input and it also determines the convergence rate of the output to D_{ref}. It is also noted that a secondary role of parameter estimation is to monitor a possible failure in the roll gap system.

3.1.3. Roll drive control

Two control objectives of the roll-speed control system are: first, the roll-speed controller should eliminate the torsional vibrations caused by the large gear ratio and the heavy roll. Second, it should also track well the reference roll speed signal generated by the high-level roll separating force controller. To achieve these two objectives, the two-degree-of-freedom robust servo controller (Youla & Bongiorno, 1985; Ohishi, Miyazaki, & Nakamura, 1996; Yi & Tomizuka, 1999) is adopted.

From (21) and (22), the following transfer function is obtained.

$$\omega(s) = G_1(s) i_a(s) - G_2(s) M(s), \quad (29)$$

where

$$G_1(s) = \frac{K_s K_T}{(J_r s + B_r)\{J_M s^2 + (K_s J_M + B_M)s + (K_s B_M + K_s)\}}$$

and

$$G_2(s) = \frac{J_M s^2 + B_M s + K_s}{(J_r s + B_r)\{J_M s^2 + (K_s J_M + B_M)s + (K_s B_M + K_s)\}}.$$

To design a robust servo controller, let $G_1(s)$ denote the plant dynamics $\hat{P}(s)$. Then, a nominal dynamics of $\hat{P}(s)$ using the coprime factorization is defined as follows:

$$\hat{P}(s) = C(sI - A)^{-1}B = N_f D_f^{-1}, \quad (30)$$

where $\{A, B, C\}$ is a realization of $\hat{P}(s)$, N_f and D_f are the coprime factorizations of $\hat{P}(s)$ (Zhou & Doyle, 1999). They must be stable and proper functions, which is designed by the state feedback gain matrix Z and the state observer gain matrix H defined as

$$N_f(s) = C(sI - A + BZ)^{-1},$$

$$D_f(s) = I - Z(sI - A + BZ)^{-1}B, \quad (31)$$

$$X(s) = I - Z(sI - A + HC)^{-1}B,$$

$$Y(s) = Z(sI - A + BF)^{-1}H,$$

where $X(s)$ and $Y(s)$ is the polynomials satisfying $N_f X + D_f Y = 1$. The following feedback controller $C_1(s)$ and feedforward controller $C_2(s)$ are determined using the coprime polynomials and the free parameters

$Q(s)$ and $K(s)$.

$$C_1(s) = \frac{X(s) + Q(s)N_f(s)}{Y(s) - Q(s)D_f(s)}, \tag{32}$$

$$C_2(s) = D_f(s)K(s) + C_1(s)\{N_f(s)K(s) - I\},$$

where the parameter $K(s)$ is arbitrarily designed by the tracking performance and another parameter $Q(s)$ is determined by the disturbance rejection performance and robust stability. Detailed developments are referred to (Youla & Bongiorno, 1985; Ohishi et al., 1996; Yi & Tomizuka, 1999). The controller parameter values used for simulations are listed in Table 2.

3.2. High-level control design

In this section, in order to regulate the roll separating force in the steady state, a robust force regulation scheme is investigated using the system identification and uncertainty quantification methods.

3.2.1. Model simplification and identification

In the steady state, if each local controller performs well, the roll gap, the molten steel level, and the roll speed can be maintained constant. The control variable for adjusting the roll separating force F could be one out of h, ω, and D. Because the strip thickness should not be altered by the high-level controller, sustaining the same h and D is desirable. Therefore, ω is picked as a parameter to be controlled for regulating the roll separating force in the steady state. Then, because h_{ref} and D_{ref} are set to constants in the steady state, only three parts, i.e. the roll drive system, the solidification process, and the roll separating force and torque from Section 2, are re-considered.

First, concerning the roll drive system, the closed loop dynamics from ω_{ref} to ω is simplified as follows:

$$\ddot{\omega} + 2\zeta\omega_n\dot{\omega} + \omega_n^2\omega = \omega_n^2\omega_{ref}. \tag{33}$$

Second, concerning the solidification process, (14) is approximated as follows:

$$\dot{T}_k \cong \frac{-\dot{\omega}T_k}{\omega - \dot{\omega}T_k + g_1(T_k)} \triangleq f(\omega, \dot{\omega}, T_k). \tag{34}$$

Note that in deriving (34) from (14), ϕ_L and D are kept constant and the following approximation has been also utilized:

$$\omega(t - T_k) \cong \omega(t) - \dot{\omega}(t)T_k. \tag{35}$$

Define the state variables as $\mathbf{x} = [\omega \quad \dot{\omega} \quad T_k]^{\mathrm{T}}$. Then, a linearized system of (33), (34), and (15) at an operating point is obtained as

$$\delta\dot{\mathbf{x}} = A\delta\mathbf{x} + B\delta\omega_{ref}, \quad \delta F = C\delta\mathbf{x}, \tag{36}$$

where

$$A = \begin{pmatrix} 0 & 1 & 0 \\ -2\zeta\omega_n & -\omega_n^2 & 0 \\ \partial f/\partial\omega & \partial f/\partial\dot{\omega} & \partial f/\partial T_k \end{pmatrix},$$
$$B = \begin{bmatrix} 0 \\ \omega_n^2 \\ 0 \end{bmatrix}, \quad C = \frac{\partial F}{\partial \mathbf{x}}. \tag{37}$$

Let $G_o(s)$ be the nominal transfer function from ω_{ref} to F. Then, $G_o(s)$ can be written as follows:

$$G_o(s) = \frac{\delta F(s)}{\delta\omega_{ref}} = \frac{b_1 s + b_0}{s^3 + a_2 s^2 + a_1 s + a_0}. \tag{38}$$

The coefficients of (38) will be estimated through experiment. Therefore, it should be observed that all the above development in Section 3.2.1 has led to only the structure of a high-level plant model, which is a third order. Now, to apply the uncertainty quantification method of Goodwin, Gevers, and Ninness (1992), a discrete model of (38) is introduced as follows:

$$G_o(z) = \frac{\delta F(k)}{\delta\omega_{ref}(k)} = \frac{b_2' z^{-1} + b_1' z^{-2} + b_0' z^{-3}}{1 + a_2' z^{-1} + a_1' z^{-2} + a_0' z^{-3}}. \tag{39}$$

In converting (38) into (39), $T_s = 0.02\,\mathrm{s}$ has been assumed. Rearranging terms of (39), the following regression form is obtained.

$$F(k) = \phi^{\mathrm{T}}(k)\theta, \tag{40}$$

where $\theta^{\mathrm{T}} = [a_2' \;\; a_1' \;\; a_0' \;\; b_2' \;\; b_1' \;\; b_0']$ and $\phi^{\mathrm{T}}(k) = [-F(k-1) \;\; -F(k-2) \;\; -F(k-3) \;\; \omega_{ref}(k-1) \;\; \omega_{ref}(k-2) \;\; \omega_{ref}(k-3)]$. Again, a recursive least squares estimation algorithm can be used to estimate θ. For the excitation signal, the sampling time, identified model, etc. are discussed in Section 3.2.4 next.

3.2.2. Uncertainty quantification

In this subsection, the uncertainty bound of the nominal model (39) is investigated, i.e., the magnitude of modeling errors of (39) in the frequency domain, which are in the form of the unstructured uncertainty resulted in deriving (33)–(36) and the structured uncertainty resulted in estimating (40), are quantified.

It is assumed that input-output experimental data are given in the following relationship.

$$y(k) = G_T(z)u(k) + v_n(k), \tag{41}$$

where $G_T(z)$ is the true transfer function and $v_n(k)$ is a stationary stochastic process, whose characteristics are

Table 2
Controller parameters used for roll drive control

Symbol	Controller parameters
C_1	$(1.69\times10^5 s^3 + 4.97\times10^7 s^2 + 3.88\times10^8 s - 1.078\times10^7)$ $/(s^4 + 2.69\times10^3 s^3 + 1.86\times10^5 s^2 + 8.49\times10^6 s + 2.74\times10^6)$
C_2	$(-2.4\times10^2 s^4 - 1.3\times10^4 s^3 - 3.3\times10^5 s^2 - 5.1\times10^6$ $s - 5.3\times10^7)/(s^5 + 79 s^4 + 2.9\times10^3 s^3 + 7.2\times10^4 s^2$ $+1.1\times10^6 s + 1.1\times10^7)$

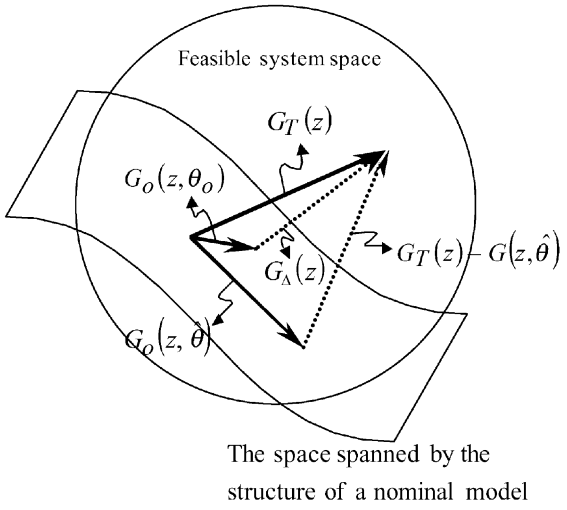

Fig. 6. A basic idea for quantifying the model uncertainty with the stochastic embedding approach.

defined by $N(0,\sigma_v)$. But, it is very difficult to know the exact true transfer function $G_T(z)$. In order to solve this difficulty, the 'stochastic embedding' approach introduced by Goodwin et al. (1992) is adopted in this work.

Let the true transfer function be denoted by

$$G_T(z) = G_o(z,\theta_o) + G_\Delta(z) \tag{42}$$

and

$$E\{G_T(z)\} = G_o(z,\theta_o),$$

where $G_o(z,\theta_o)$ is a nominal model of $G_T(z)$ with nominal parameter θ_o, $G_\Delta(z)$ is a neglected part of $G_T(z)$ in the form of additive uncertainty, and E denotes the expectation over a stochastic process. θ_0 is replaced by its estimate $\hat{\theta}$ in practice.

As depicted in Fig. 6, the "feasible system space" refers to the space on which the real transfer function $G_T(z)$ lies. In addition, the essential capability for the estimated nominal model $G_o(z,\hat{\theta})$ to represent $G_T(z)$ is restricted according to the space spanned by the structure of a nominal model. Then, the uncertainty of an estimated transfer function, i.e., $G_o(z,\hat{\theta}) - G_T(z)$, is composed of a structured uncertainty $G_o(z,\hat{\theta}) - G_o(z,\theta_o)$ and an unstructured uncertainty $G_\Delta(z)$.

Another way of representing the model error is the form of multiplicative uncertainty. Let the true transfer function of the plant be defined in the following form:

$$G_T(z) = G_o(z,\hat{\theta})(1 + \Delta(z)), \tag{43}$$

where $\Delta(s)$ denotes the multiplicative uncertainty. From (43), the following relationship is derived:

$$|\Delta(s)|^2 \approx E\{|\Delta(z)|^2\} = \frac{E\left\{\left|G_T(z) - G_o(z,\hat{\theta})\right|^2\right\}}{\left|G_o(z,\hat{\theta})\right|^2} \tag{44}$$

for all $\omega \leqslant \pi/T_s$,

where $\Delta(s)$ denotes the uncertainty of the continuous model and T_s is the sampling time. Because $G_o(z,\hat{\theta})$ in the denominator of (44) is known, the uncertainty quantification problem now becomes the problem of finding the magnitude bound of $G_T(z) - G_o(z,\hat{\theta})$. In estimating $E\{|G_T(z) - G_o(z,\hat{\theta})|\}$, the estimation sequence summarized from the work of Goodwill et al. (1992) is utilized, see Section 4 of Hong and Kim, 1999 and Section 5 of Hong, Kim, and Lee, 1999.

3.2.3. High-level control: H_2 optimal controller

Consider the feedback configuration depicted in Fig. 7, where $G_o(s,\hat{\theta}_N)$ is the transfer function given in (38), which is obtained by transforming (39) back to the continuous time domain, and $\Delta(s)$ is a multiplicative uncertainty comprising both the structured and unstructured uncertainty. Then, the robust stability and robust performance criteria for the multiplicative uncertainty of (44) are given by

$$|\Delta(j\omega)T(j\omega)| < 1 \quad \text{for all } \omega, \tag{45}$$

$$|W(j\omega)S(j\omega)| < 1 \quad \text{for all } \omega, \tag{46}$$

where $T(j\omega) = G_o(j\omega,\hat{\theta})K(j\omega)(1 + G_o(j\omega,\hat{\theta})K(j\omega))^{-1}$ is the complementary sensitivity function and $S(j\omega) = (1 + G_o(j\omega,\hat{\theta})K(j\omega))^{-1}$ is the sensitivity function (Doyle, Francis, & Tannenbaum, 1992).

An H_2 optimal solution of (45) and (46) in the framework of LQG/LTR is given by

$$K_{opt}(s) = K_c(sI - \hat{A} - \hat{B}K_c - K_f\hat{C})^{-1}K_f, \tag{47}$$

where $\hat{A}$, $\hat{B}$, and $\hat{C}$ consist of the estimated parameters, K_f and K_c are the LQG/LTR gains (Stein & Athans, 1987). The selection of K_f and K_c is as follows: First, design a target feedback loop to satisfy (45) with the uncertainty bound (44). Then, obtain the robust optimal control gains by following the cheap control method (Stein & Athans, 1987).

3.2.4. Controller example

A full-scale experimental data of the strip casting process is not yet available. This new method is still under development. A complete production line, except a laboratory-scale partial pilot plant, has not been constructed yet. However, an artificial data, for the purpose of verifying the methodologies developed in this

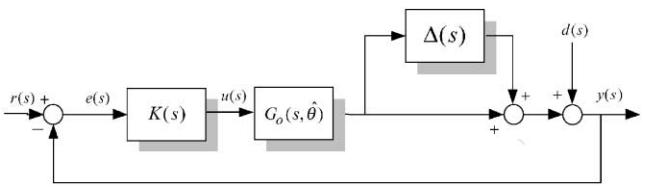

Fig. 7. A feedback configuration with the multiplicative model uncertainty and output disturbance.

paper, has been generated using the nonlinear equations derived in Section 2. Twenty thousand output data for 20 s, assuming that this is continuous data from a real plant, were made up for system identification purpose. It is also noted that a measurement noise of zero mean and $\sigma_v = 0.005$ has been added to the output signal. The output data generation part is the only fictitious work in this paper.

One thousand points out of twenty thousand data, assuming sampling time $T = 0.02$ s, has been collected. By following the procedure discussed in Section 3.2.1, an estimated nominal transfer function of (39) is finally obtained as follows:

$$G_o(z) = \frac{-0.472z^2 - 0.0549z - 0.062}{z^3 - 0.247z^2 - 0.236z - 0.245}. \quad (48)$$

Hence, transforming (48) back to the continuous time domain using the bilinear transformation with $T_s = 0.02$ sec yields:

$$G_o(s) = \frac{0.384s^3 + 27.14s^2 - 1840s - 468900}{s^3 + 218.8s^2 + 29650s + 21660}. \quad (49)$$

The bandwidth of the Bode diagram of (48) is about 9 rad/s (1.43 Hz).

The upper plot in Fig. 8 shows a persistently exciting input signal used for identification, i.e. $\omega_{ref}(t) = 3 + 0.9\sin(t) + 0.4\sin(3t) + 0.01\sin(0.5t)$. The lower plot compares the twenty thousand raw data and the time domain response of (49). It is observed that the overall trend agrees well. Therefore, under the assumption that the artificial data is the real one obtained from the strip casting process, the procedures in this paper are justified. The discrepancy between these two plots would be due to the neglected dynamics and parametric uncertainties as discussed in Section 3.2.2.

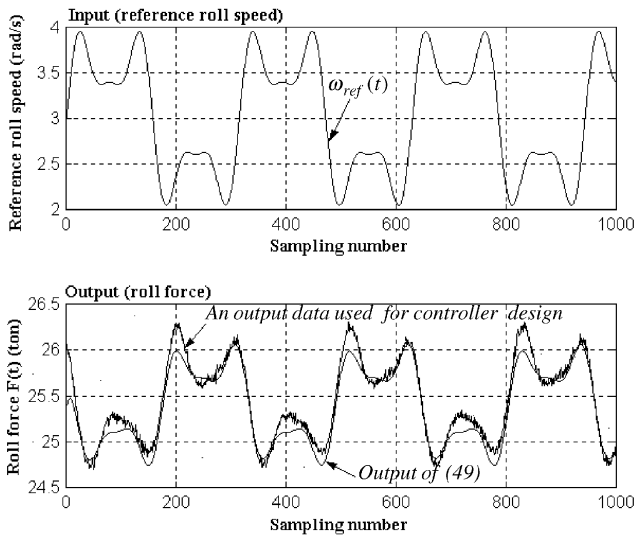

Fig. 8. Comparison between a raw data for system identification and the response of (49).

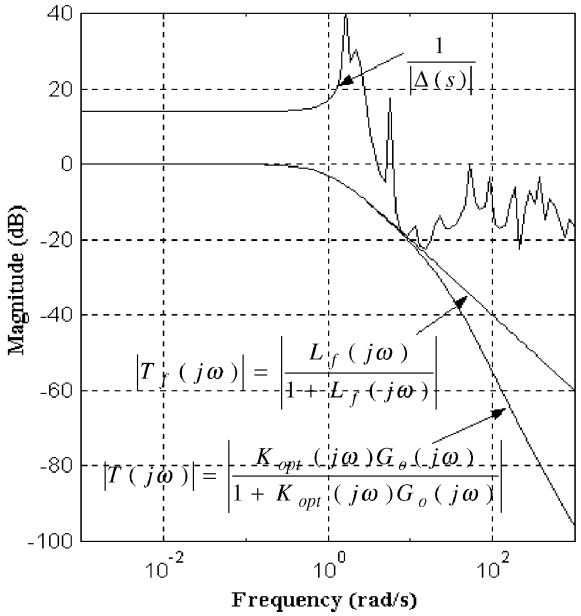

Fig. 9. A design example of robust H_2 optimal control.

The upper curve of Fig. 9 illustrates the inverse of $E\{|\Delta(z)|\}$ obtained through (44). The lower magnitude plots are the closed loop transfer functions of the controlled system and the target feedback loop (L_f), respectively. It should be observed that the robust stability criterion (45) is satisfied. Finally, the robust H_2 optimal controller $K_{opt}(s)$ is derived in the following form:

$$K_{opt}(s) = \frac{-3.162s^3 - 3557s^2 - 1.614\times10^7 s - 2.153\times10^8}{s^4 + 1135s^3 + 5.115\times10^6 s^2 + 1.193s + 9.85\times10^8} \quad (50)$$

with the weighting function $W(s)$ of (46) selected by

$$W(s) \approx \frac{1}{s}. \quad (51)$$

4. Simulations

In Figs. 10 and 11, the start-up operation, the performance of the high-level supervisory controller, and the rejection of a unit magnitude disturbance of roll force that occurs during 30–60 s are simulated. When the start-up operation ends at around 10 s, it is observed in Fig. 10 that the roll gap, the molten steel level, and the roll speed are maintained at their desired values. However, as seen in the upper plot of Fig. 11, the roll force is still fluctuating. Therefore, the high-level controller is turned on at 20 s. Then, with the adjustment of the roll speed, the roll force is now maintained at its desired level. Now, at 30 s, a unit magnitude disturbance

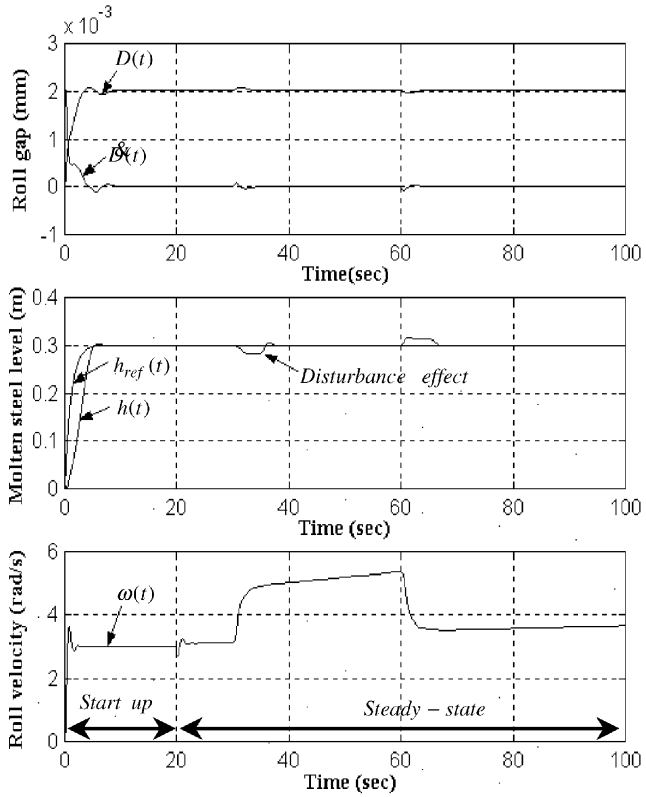

Fig. 10. Simulations of the roll velocity, the molten steel level, and the roll gap.

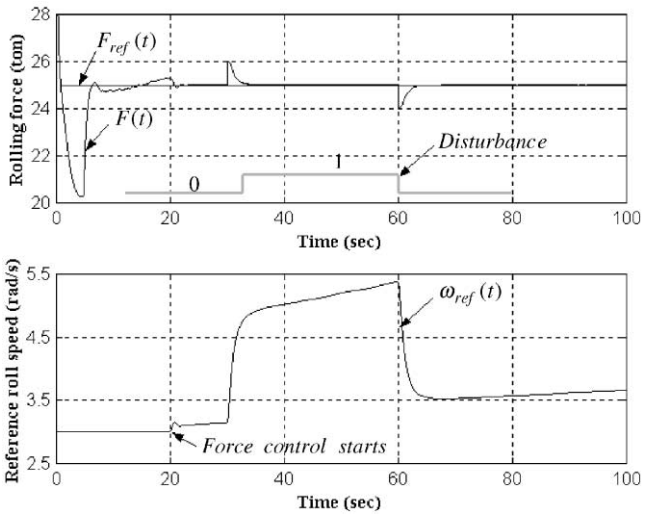

Fig. 11. The performance of roll separating force control and disturbance rejection: high-level control.

of roll force is inserted for 30 s, as shown in the upper plot of Fig. 11. Then, the disturbance rejection of the high level controller is well illustrated in the roll gap and roll force diagrams by providing a new reference signal to the local roll-speed controller as depicted in the lower plot of Fig. 11.

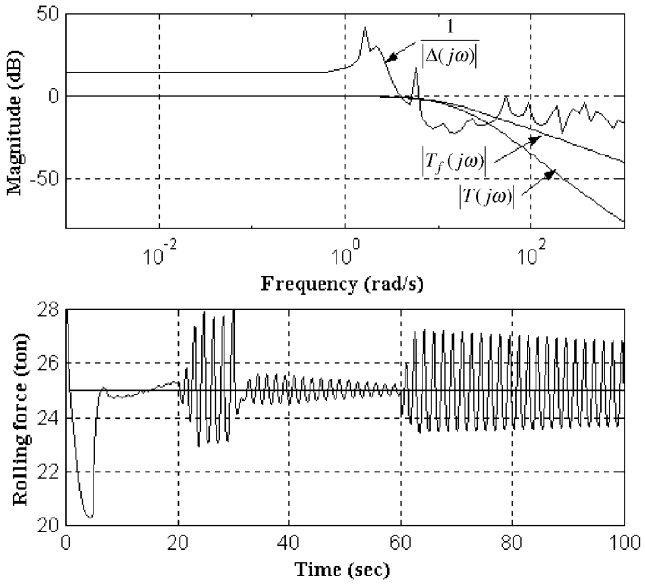

Fig. 12. A counter example that does not satisfy (45) and its control performance.

As a counter example, i.e., a controller that violates (45) as shown in the upper plot of Fig. 12, has been selected and simulated. The local controllers have demonstrated the same behavior, but as shown in the lower plot of Fig. 12 the roll force has never been stabilized.

5. Conclusions

In this paper, the modeling and control of a strip caster was investigated. Mathematical models for the strip casting process were obtained by analyzing five critical areas: the molten steel level, the solidification process, the roll separating force and torque, the roll gap dynamics, and the roll drive dynamics. A two-level control strategy was proposed: three low-level controllers include a variable structure controller for the molten steel level in the pool, an adaptive one step ahead predictive controller for the roll gap, and a robust servo controller for the roll drive system. At high-level, the roll separating force controller, which is robust to model uncertainties, was proposed using the uncertainty quantification method.

A full-scale experimental setup is not yet available at the current stage. The paper has suggested, however, the overall control structure and the most adequate control methodology for each of the control loops introduced in the system. The authors believe that the model and control scheme discussed in the paper provide a useful guideline to determine the entire control system configuration of the strip casting process and to provide an idea for handling the complex nonlinear MIMO system.

Acknowledgements

This work was supported in part by the Korea Research Foundation under Grant KRF-1998-001-E00198. The second author was supported in part by the Brain Korea 21 Program of the Ministry of Education and Human Resources, Korea.

References

Astrom, K. J., & Wittenmark, B. (1995). *Computer controlled systems*. Englewood Cliffs, NJ: Prentice-Hall.

Bernhard, S., Enning, M., & Rake, H. (1994). Automation of a laboratory plant for direct casting of thin steel strips. *Control Engineering Practice*, *2*(6), 961–967.

Doyle, J. C., Francis, B. A., & Tannenbaum, A. R. (1992). *Feedback control theory*. New York: Maxwell Macmillan, 1992.

Garimella, S. S., & Srinivasan, K. (1996). Application of repetitive control to eccentricity compensation in rolling. *ASME Transactions Journal of Dynamic Systems, Measurement, and Control*, *118*(4), 657–664.

Goodwin, G. C., Gevers, M., & Ninness, B. (1992). Quantifying the error in estimated transfer function with application to model order selection. *IEEE Transactions on Automatic Control*, *37*(7), 913–927.

Graebe, S. F., Goodwin, G. C., & Elsley, G. (1995). Control design and implementation in continuous steel casting. *IEEE Control Systems Magazine*, *15*(4), 64–71.

Hesketh, T., Clements, D. J., & Williams, R. (1993). Adaptive mould level control for continuous steel slab casting. *Automatica*, *29*(4), 851–864.

Hong, K. S., & Kim, S. H. (1999). Robust time-delay control of a reclaimer. *KSME International Journal*, *13*(7), 575–583.

Hong, K. S., Kim, S. H., & Lee, K. I. (1999). Reclaimer control: kinematics, modeling, identification, and robust Smith predictor. *Proceedings of the 14th World Congress of IFAC*, Beijing, China, July 5–9, Preprint Number N-7b-01-6, Vol. N (pp. 409–414).

Lee, D., Lee, J. S., Kim, Y. H., & Lee, D. S. (1996). Modeling and stable startup strategy for strip-caster. *Proceedings of the 11th Korea Automatic Control Conference*, Seoul, Korea (pp. 319–322).

Ljung, L. (1987). *System identification: Theory for the user*. Englewood Cliffs, NJ: Prentice-Hall.

Manayathara, T. J., Tsao, T.-C., Bentsman, J., & Ross, D. (1996). Rejection of unknown periodic load distrubance in continuous steel casting process using learning repetitive control approach. *IEEE Transactions on Control Systems Technology*, *4*(3), 259–265.

Ohishi, K., Miyazaki, T., & Nakamura, Y. (1996). High performance ultra low speed range based on doubly coprime factorization and instantaneous speed observer. *IEEE/ASME Transactions on Mechatronics*, *1*(1), 89–98.

Pietrzyk, E., & Lenard, J. G. (1991). *Thermal-Mechanical Modeling of the Flat Rolling Process,* Berlin, Heidelberg: Springer.

Phillips, C. L., & Nagle, H. T. (1997). *Digital control system analysis and design*. Englewood Cliffs, NJ: Prentice-Hall International, Inc..

Slotine, J. J. E., & Li, W. (1991). *Applied nonlinear control*. Englewood Cliffs, NJ: Prentice-Hall.

Stein, G., & Athans, M. (1987). The LQG/LTR procedure for multivariable feed-back control design. *IEEE Transactions on Automatic Control*, *32*(2), 105–114.

Yi, L., & Tomizuka, M. (1999). Two-degree-of-freedom control with robust feedback control for hard disk servo systems. *IEEE/ASME Transactions on Mechatronics*, *4*(1), 17–24.

Youla, D. C., & Bongiorno Jr., J. J. (1985). A feedback theory of two degree-of-freedom optimal Wiener-Hopf design. *IEEE Transactions Automatic Control*, *AC-30*(7), 652–665.

Zhou, K., & Doyle, J. C. (1999). *Essentials of robust control*. Englewood Cliffs, NJ: Prentice-Hall International, Inc.